Bragg gratings in multimode optical fibres and their applications

Xinzhu Sang, Chongxiu Yu, Binbin Yan

Key Laboratory of Optical Communication and Lightwave Technologies, School of Electronic Engineering, Beijing University of Posts and Telecommunications, Beijing,100876 China

Spectra evolutions of Bragg gratings written in the step-index multimode optical fibre are analyzed and investigated experimentally, which show that different kind gratings can be achieved with different irradiation pulses. Applications of multimode fibre Bragg gratings to optical sensing and optical communications are discussed. A chemical sensor based on an etched multimode fibre Bragg grating is demonstrated experimentally.

1. Introduction

Since the discovery of photosensitivity in germanium-doped silica fibre, fibre Bragg gratings (FBGs) in single-mode fibre have been studied extensively, and their formation dynamics, spectral characteristics have been well known [1-2]. At present, they have are increasingly becoming important devices in optical communications, optical sensing and signal processing. Multimode fibres (MMFs) offer more flexibility in grating design and performance characteristics compared to single-mode fibre, since the spectral response may be tuned by core size, numerical aperture and mode coupling characteristics of the gratings. In addition, multimode fibres have a merit of easy coupling with inexpensive light sources and other optical components due to their large core, so gratings in multimode are preferred to yield lower cost systems. Therefore, Bragg gratings in multimode fibres have also received attention in recent years. Wanser *et al.* [3] first calculated the theoretical spectrum of a Bragg grating in MMF, showed multiple peaks and proposed applications to bending sensors. Mizumami *et al* [4] experimentally investigated the spectral characteristics of Bragg gratings in graded-index MMF and an analysis of grating behavior including excitation condition of propagating modes, temperature and polarization characteristics. Zhao *et al.* [5] fabricated a Bragg grating in a multimode fibre by phase mask technique whose spectrum was similar to than of Bragg gratings in single-mode fibres, and its temperature and strain responses were analyzed. Szkopek *et al.* [6] proposed a novel multimode fibre structure with modal propagation characteristics and tailored to facilitate the creation of narrowband high reflectivity Bragg gratings, and this group[7] later demonstrated gratings with reflectivity of >98% and bandwidths of <0.5 nm at ~1550 nm in this fibre. Lim *et al* [8] fabricated two Bragg gratings sensors in 62/125 μm graded-index multimode fibre by the holographic method and phase mask technique respectively for application in a power-by-light hydraulic valve monitoring system. Zhou *et al* [9,10] reported two-dimensional optical power distribution of side-out-coupled radiation and side detection of strong radiation-mode out-coupling from tilted FBGs in multimode fibre, and Yang *et al* [11] observed that there were two different wavelength group in the transmission spectrum of tilted Bragg gratings in multimode fibre as the tilted angle was between $2.5°$ and $4°$. Liu *et al* [12] demonstrated a comb filter based Bragg gratings in graded-index multimode fibre. Recently, we have investigated growth dynamics of Bragg gratings in the multimode optical fibre [13].

In this paper, we will analyze theoretical background and describe detailed spectra evolutions of Bragg gratings written in step-index MMFs by phase mask technique. Applications of multimode fibre Bragg gratings to optical sensing and optical communications are discussed. A multimode fibre Bragg grating chemical sensor is demonstrated experimentally

2. Theoretical background

A step-index multimode optical fibre carries many modes with different velocities and exhibit different mode field profiles, and the maximum number of propagating modes in it is usually calculated by the equation

$$M \approx \frac{V^2}{2} = \frac{2\pi^2 a^2}{\lambda^2}(n_1^2 - n_2^2) = \frac{2\pi^2 a^2}{\lambda^2}NA^2 \qquad (1)$$

where V is normalized frequency, a is core radius, NA is numerical aperture, λ is operating wavelength, n_1 and n_2 are core refractive index and cladding refractive index respectively. However, some modes can propagate in the fibre core with the same propagation constant, and the modes with the same propagation can be classified into the same principal modes. These modes exchange energy inside the fibre core. As they reach the Bragg grating, those modes satisfying the phase-matching conditions will be reflected, and several transmission dips in the transmission spectra will be created because they have different propagation constants.

The phase-matching condition of a uniform Bragg grating with the period Λ is give by $\beta_i - \beta_j = 2\pi/\Lambda$, where β_i and β_j are the propagation constants of forward and backward propagating modes. For reflection to the same mode, $\beta_j = -\beta_i$. For step-index multimode fibre, the propagation constant for the Kth principal mode is given by [14]

$$\beta_K = \frac{2\pi}{\lambda} \left[n_2^2 + b_K NA^2 \right]^{1/2} \qquad (2)$$

where b_K is the normalized propagation constant for the Kth principal mode, which is determined by

$$V = \frac{1}{(1-b_K)^{1/2}} \left[K\pi/2 + \pi/4 + \arctan\left(\frac{b_K}{1-b_K}\right)^{1/2} \right] \qquad (3)$$

So the location of transmission dips can be determined approximately by propagation constants and the grating period. The width of the separations between the resonance peaks can be reduced or increased as desired by changing the fibre waveguide profiles; this feature may be applied in designing a multi-wavelength filter. In the writing process of the grating, the average refractive index increase and the propagation constants will change too, so the transmission dips will shift to the red. In addition, new transmission dips appeared because the phase matching condition of a new mode was nearly satisfied, and it disappeared again because of its imperfect phase matching with further irradiation. The total bandwidth obtained by the combined several resonance peaks is significantly greater that that of any one of them, thus yielding the wide-band filter.

The coupled-mode theory can be employed to investigate the grating properties in the multimode fibre. The total electric field can be expanded in terms of the electric fields of fibre modes. In the absence of the Bragg gratings, for given mth mode propagating in the z direction, its mode amplitude obeys the following coupled-mode equations [23]

$$\frac{dA_m}{dz} = \sum_{n \neq m} -iK_{mn} \exp\left[-i\left(\beta_n - \beta_m + \frac{2\pi}{\Lambda} \right)z \right] A_n \quad (4)$$

where A_m is the mode amplitude of mth mode, β_n the propagation constants and K_{mn} and Λ are the coupling coefficient between modes m and n and grating period. If the detuning $\beta_m - \beta_n - 2\pi/\Lambda$ is near zero (that is say that phase matching condition is satisfied), the modes are strongly coupled. The coupling strength depends on the coupling coefficient between modes m and n. If the modes m and n propagate in the same direction, then $K_{mn} = K_{nm}^*$, otherwise, if the modes propagate in opposite directions, $K_{mn} = -K_{nm}^*$. K_{mn} is defined by [24]

$$K_{mn} = \frac{\omega}{4} \iint \Delta\varepsilon(x,y,z) \vec{e}_m(x,y) \cdot \vec{e}_n^*(x,y) dx dy \qquad (5)$$

where $\triangle \varepsilon$ is the perturbation to the permittivity, approximately $\triangle\varepsilon \approx 2n\delta n$ when $\delta n << n$, ω is the optical frequency, $e_m(x,y)$ and $e_n(x,y)$ are the electric field distribution of the modes m and n normalized to unit power.

It is noted that the reflected wave and incident wave for the same mode are considered as different modes equation (4). The phase matching condition must be meet for the modes to efficiently coupled incident to reflected fibre modes. If the modes in the fibre don't exchange energy among them, each mode can be described by an incident and a reflected wave. Besides the coupling of the incident and reflected waves for mth fibre mode, the coupling between the incident wave of pth fibre mode and the reflected wave of the qth fibre mode can also occur. The transmission dip in the long wavelength side may become broad with exposure pulse number increasing due to two reasons:(1) for the same principal mode, the modulation depth become larger with further irradiation; (2) the coupling of between different modes of opposite propagating directions occurs and overlaps with the coupling of the reflected wave and incident wave for the same principal mode. In this process, the coupling between the modes with different principle modes occur, so there are many ripples in the floor of the transmission dip. Moreover, the coupling strength for them can become stronger or poorer sometimes, so there are increase and decrease for the transmission loss in some locations.

The discussion above for the uniform Bragg grating can also be applied to tilted Bragg gratings. The main effect of the tilt angle in a Bragg grating is to reduce the coupling of between the forward and backward waves. Moreover, the tilt angle can also dramatically affect the coupling to radiation modes and cladding modes. When the guided modes reaching the grating, some modes will coupled to other guided, radiation and cladding modes according to phase matching condition. They will create some dips in the transmission spectrum. It can be shown that the Bragg wavelength λ_{ijB} due to the coupling between the forward traveling core mode and the backward traveling cladding mode is given by [16]:

$$\lambda_{ijB} = \frac{\left[n_{i\,eff} + n_{j\,cl}\right]\Lambda_g}{\cos\theta} \qquad (6)$$

where n_{cl} is the refractive index of the cladding and θ is the tilt angle. When the tilt angle is small, there is essentially an overlap of the transmission spectra between the core-core mode coupling and the core-cladding mode coupling. Hence the corresponding dip amplitude increases. During exposure process, the effective index of each core mode increases resulting in the broadening of its stop band in exactly the same manner as in the case of untilted grating. The transmission dip due to the core-cladding mode coupling widens. This gives rise to the overlap of the composite spectrum. As the tilt angle increases further the Bragg wavelength due to coupling between the core mode and the cladding mode deviates more from the untilted Bragg wavelength as indicated in Eq.(6). Hence some ripples may appear in the stop band of the transmission spectra.

3. Formation of Bragg gratings in the step-index MMF

The schematic of experimental setup for fabricating Bragg gratings used in this work is shown in Fig. 1. The ultraviolet (UV) light source is a narrowband KrF excimer laser operating at 248 nm, whose output energy density per pulse and repetition rate can be controlled with a computer. The repetition rate of output pulses and energy density per pulse are set to 10 Hz and 140 mJ respectively in our experiments. The UV beam is expanded by a beam expander first and directed by a mirror into the phase mask and focused with a cylindrical lens onto the fibre. The beam dimensions at the fibre are about 4 mm ×1.5 mm. The uniform phase mask is designed to suppress the amount of light that is diffracted into the zeroth -order beam(<2.9% at 248 nm). The dimensions of the phase mask used in the experiment are 20 mm ×5 mm and it has a period of 1064 nm. The rotating plate is used to adjust the tilted angle between fibre axis and the phase mask. The grating growth can be monitored in real time during inscription process by launching broadband light near 1550 nm from an EDFA into the fibre and an optical spectrum analyzer.
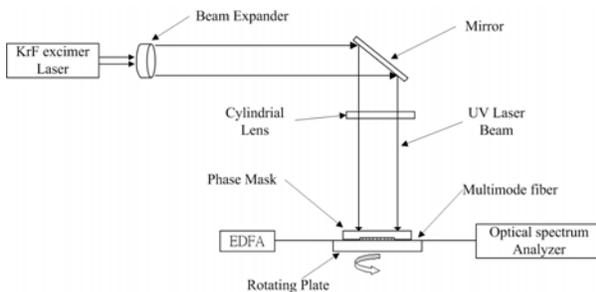

Fig.1 Schematic of experimental setup for fabricating multimode fibre Bragg grating at different tilt angles.

Standard step-index MMFs with a core diameter of 50 μm and a numerical aperture of 0.22 were used for fabrication of Bragg gratings. Before writing grating in the fibre, the fibre was sensitized by hydrogen loading for 11 days at a pressure of 100 atm. We fabricated three Bragg gratings with the same phase mask at different tilted angles. In the writing processes, transmission spectra were recorded at the intervals of 200 pulses.

The transmission spectra of a uniform Bragg grating resulting from irradiating a different number N of the 248nm pulses are shown in Fig. 2. We call this the regular grating because its axis coincides with the axis of the fibre, i.e. there is no tilt. When the fibre is irradiated by 800 pulses, three transmission dips appear at wavelengths 1554.78nm, 1553.85nm and 1553.82nm respectively, indicating that three propagating modes are reflected by the grating. As the number of irradiating pulses increases, the Bragg wavelength for each mode shifts towards long wavelength, i.e. a red shift. This is also accompanied by the broadening of the spectrum. New transmission dips also emerge at the short wavelength side. As the number of irradiation pulses increases beyond 2400, the width of each dip increases rapidly and they tend to overlap each other. As theoretical analysis, there are several noticeable features in transmission spectra in this process: (1) new transmission dips appeared and disappeared again in the short wavelength side; (2) the bandwidth of the maximum transmission dip in the long wavelength side became broad rapidly; (3) the two transmission dips in the long wavelength side emerged into one and a broad band-stop filter with bandwidth of 2.2 nm formed; (4) there were some ripples in the bottom of the broad transmission dip.

Tilted Bragg gratings were formed in step-index multimode fibres by adjusting the rotating plate shown in Fig. 1. Again, we monitored the growth of the Bragg spectrum as the number N of the irradiation pulses increases. Fig.3 shows the Bragg spectra when the tilt angle is 0.6°. Since the tilt angle is small, the transmission spectra shown in Fig.3 closely resemble those shown in Fig. 2. However, there is a slight increase in the amplitude of each dip indicating more transmission power loss, especially for higher order modes. As the number of irradiation pulses increases, the effective index of each core mode increases resulting in the broadening of its stop band in exactly the same manner as in the case of untilted grating. In fact, the stop band due to the core-cladding mode coupling widens. This gives rise to the overlap of the composite spectrum.
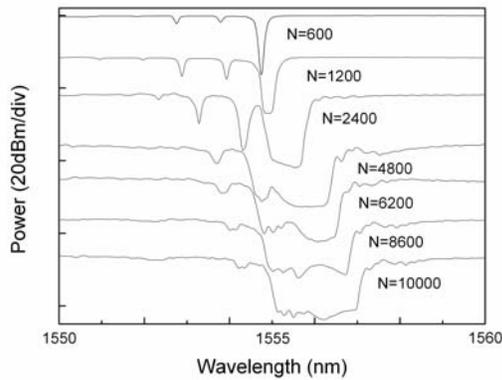
Fig. 2. Transmission spectra evolution of regular Bragg gratings under increasing number of irradiation pulses.
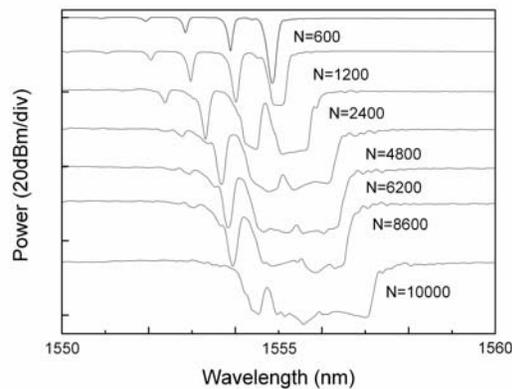

Fig. 3. Transmission spectra of tilted Bragg grating with tilt angle of 0.6°.

As the tilt angle increased to 1.2° shown in Fig. 4, more transmission dips appeared and they shifted to the red related to the uniform and 0.5° gratings with the same exposure pulse number. Since the tilt angle is small, the transmission spectra shown in Fig. 3 closely resemble those shown in Fig. 2. With exposure pulse number increasing, the bandwidth of three dips in the long wavelength become large rapidly, and the transmission loss of the forth dip becomes larger. The depth of each main dip is smaller than that in uniform and 0.6° grating. This means that the transmission dips are due mainly to the coupling of the forward and backward core modes of the same kind. However, there is a slight increase in the amplitude of each dip indicating more transmission power loss, especially for higher order modes. As the number of irradiation pulses increases, the effective index of each core mode increases resulting in the broadening of its stop band in exactly the same manner as in the case of untilted

grating. In fact, the stop band due to the core-cladding mode coupling widens. This gives rise to the overlap of the composite spectrum.
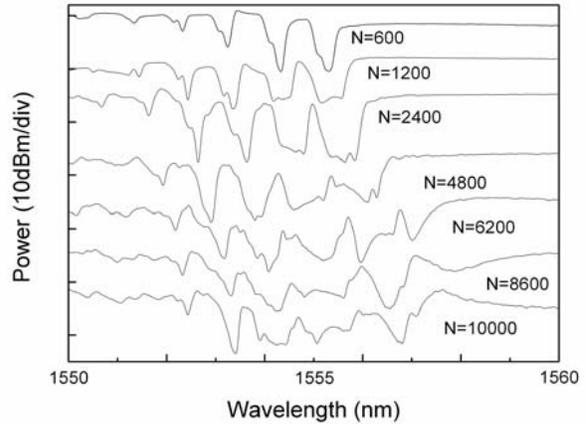

Fig. 4. Transmission spectra of a tilted Bragg grating with tilt angle of 1.6°.

As the tilt angle increases further as shown in Fig. 4 (θ=1.6°), the Bragg wavelength due to coupling between the core mode and the cladding mode deviates more from the untilted Bragg wavelength. Hence some ripples begin to appear in the stop band of the transmission spectra. As the number of irradiation pulses increases, the effect of core-cladding mode coupling becomes stronger and the ripples are more pronounced. The Bragg wavelength also shifts toward longer wavelength as N increases.

4. Applications of Bragg gratings in the step-index MMF

Recently, applications of Bragg grating have attracted people's attentions. According to spatial-mode distribution in the MMF, a wavelength-switching erbium-doped fibre laser is demonstrated [17-18]. By varying spatial-launching position of the Bragg grating in the MMF to achieve different mode group excitation and selection, single-wavelength lasing at 31 discrete wavelengths has been realized over 25 nm. With a multimode fibre Bragg grating, the oscillation wavelength of semiconductor lasers can be selected by adjusting the laser diode and multimode fibre [19-20]. Wavelength locking with high output power and narrow linewidth can be realized. Multimode fibres are used predominantly in local area networks because of their merits [21-22], multimode fibre Bragg gratings are expected to realize some key functional devices. Due to multi-peaks and their

response to different parameters, multi-parameters sensing can be realized with Bragg gratings in MMFs[8, 23]. Here, we demonstrated a multimode fibre Bragg grating(FBG) chemical sensor by etching the cladding out.
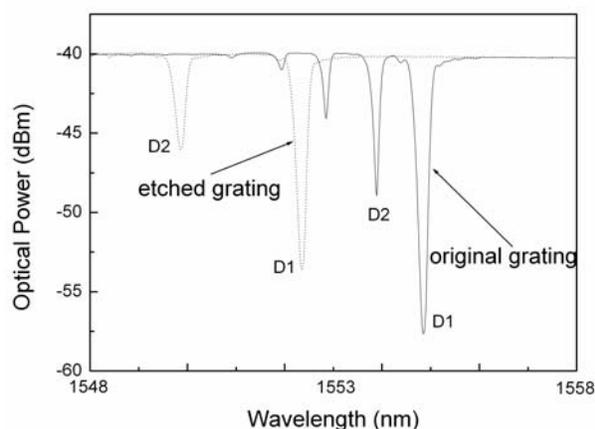

Fig. 5. Transmission spectra of original and etched multimode FBG.
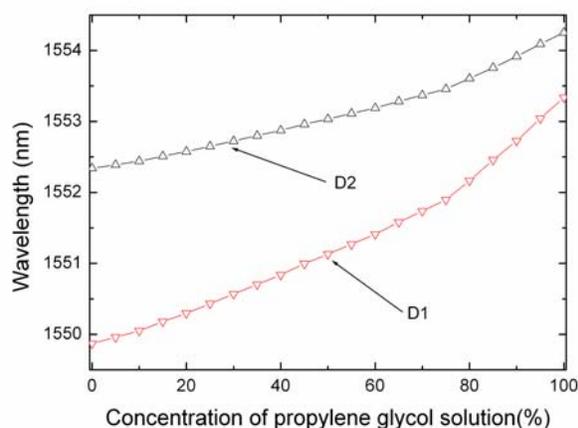

Fig. 6. Wavelength shift versus concentration of propylene glycol solution.

The principle of Bragg gratings sensing operation relies on the dependence of the Bragg wavelength on the grating period and effective index. Since the light coupling takes place only between well-bound core modes that are screened from the influence of the surrounding-medium refractive index (SRI) by the cladding, normal FBGs are intrinsically insensitive to SRI. However, if fibre cladding is reduced along the grating region, the effective refractive index is significantly affected by external refractive index. As a consequence, shifts in the Bragg wavelength

combined with a modulation of the reflected amplitude are expected. Recently, some SRI sensors employing FBGs in standard and D-shape single-mode fibres sensitized by Hydrofluoric (HF) acid etching and side-polishing techniques have been proposed[24-25]. We fabricate a Bragg grating in the multimode fibre, whose spectrum is shown by the solid line in Fig.5. The grating region is etched by 45% HF solution until the core size is reduced to about 16 μm. The spectrum of the etched grating in purified water at room temperature is given by dot line in Fig. 5. In order to characterize the chemical sensitivity of the multimode FBG, aqueous propylene glycol solutions at different concentration are used as external media. The propylene glycol solutions with concentrations ranging from 0 to 100 % are prepared in the lab. The FBG were immersed in turn into each propylene glycol solution, and their wavelength shift is measured. Fig.6 shows the sensing characteristics of the FBG. It is clear from that the two transmission dips of the FBG shift to the red with increasing the solution concentration and the transmission dip P2 a much higher concentration sensitivity than P1. If we define the concentration sensitivity as the wavelength shift change induced by 1% concentration change, we have gotten sensitivities of 0.013 and 0.026 nm/% for D1 and D2 at low concentration, and of 0.026 and 0.054 nm/% at high concentration, respectively. For FBG wavelength demodulation, several low-cost FBG interrogation modules with 1-pm resolution have been proposed. Thus, for practical applications, up to 0.04% concentration change in propylene glycol solution can be detected by this sensor with P2. The sensor can be used to detect chemical or biological changes in the surrounding medium. Multiple sensors can also be integrated on a single fibre allowing for different detection scenarios. These sensors can be used for medical, pharmaceutical, industrial fluid, petrochemical plastic, food and beverage industry applications.

5. Conclusions

In this paper, we investigated experimentally the evolution of spectral characteristics of the regular Bragg grating and tilted Bragg grating in step-index MMF during the writing process. We found that the spectral characteristics of Bragg gratings in step-index MMF could be controlled by the exposure pulse number. So it provides a flexible means to fabricate desired grating in MMF. Tilt angle can reduce coupling between forward and backward waves, but it can dramatically enhance the coupling to

irradiation and cladding modes. Some applications of Bragg gratings in MMF are discussed and a multimode fibre Bragg grating chemical sensor is demonstrated experimentally. Bragg gratings in MMF add flexibility in design and fabrication. Based on the experimental results, they maybe have merits in the in design of multiple wavelength laser and sensing systems. With further research, more applications of them are believed to be explored in optical sensing and communication systems.

References

[1] T. Erdogan, J. Lightwave Technol. **15**, 1277(1997)
[2] X. Z. Sang, P. L. Chu, C. X Yu, R. Lai, Opt. Commun. **251**, 94 (2005).
[3] K. H. Wanser, K. F.Voss, A. D. Kersey, Proc. SPIE **2360**, 265(1994).
[4] T. Mizunami, T. V. Djambova, T. Niiho, S. Gupt, J. Lightwave Technol. **18**, 230(2000).
[5] W. Zhao, R. O. Claus, Smart Mater. Struct. **9**,212(2000).
[6] T. Szkopek, V. Pasupathy, J. E.Sipe, P. W. E. Smith, IEEE J. Selected Top. Quantum Electron. **7**, 425(2001).
[7] Y. Sun, T. Szkopek, P. W. E. Simith, Opt. Commun. **233**, 94(2003).

[8] J. Lim, Q. Yang, B. E. Jones, P. R. Jackson, IEEE Trans. Instru. & Meas. **51**, 622 (2002).
[9] K. Zhou, G. Simpson, X. Chen, L. Zhang, I. Bennion. Electron. Lett. **39**, 651 (2003).
[10] K. Zhou, A. G. Simpson, L. Zhang, I.Bennion, IEEE Photon. Technol. Lett.**15**, 936 (2003).
[11] X. Yang, C. Zhao, J. Zhou, X. Guo, J. Gg, X. Zhou, C. Lu, Opt. Commn. **229**, 161 (2004).
[12] Y. Liu, J. Lit, X. Gu, L. Wei, Opt. Express **13**, 8508 (2005).
[13] X. Z. Sang, Pak L. Chu, Chongxiu Yu, Robust Lai, Opt. Commun. **260**, 131 (2006).
[14] A.Ghatak, K. Thyagarajan, Introduction to fibre optics. ch.8. Cambridge: Cambridge University Press (1998).
[15] E. Peral, A. Yariv, J.Lightwave Technol. **17**, 942 (1999).
[16] R. Kashyap, Fibre Bragg Gratings. Ch.2, New York:Academic Press (1999).
[17] L. Su, C. Lu, J. Hao, Z. Li, Y. Wang, IEEE Photon. Technol. Lett. **17**, 315 (2005).
[18] L. Su, C. Lu. Electron. Lett. 41, 11 (2005).
[19] H. G. Yu, Y. Wang, C. Q. Xu, A. D. Vandermeer, Opt. Express **13**, 1661 (2005).
[20] H. G. Yu, Y. Wang, C. Q. Xu, J. Wojcik, P. Mascher, J. Quantum Electron. **41**, 1492 (2005).
[21] X. J. Gu, W. Mohammed and P.W. Smith, IEEE Photon. Technol. Lett. **18**, 244 (2006).
[22] C. Carlsson, A. Larsson, A. Alping, J. Lightwave Technol. **22**, 1694 (2004).
[23] T. V. Djambova, T. Mizunami, Jpn. J. Appl. Phys. **39**, 1566 (2000).
[24] W. Liang, Y. Huang, Y. Xu, R. K. Lee, A. Yariv. Appl. Phys. Lett., **86**, 1551122 (2005).
[25] K. Zhou, X. Chen, L. Zhang, I. Bennion, Electron. Lett. **40**, 232 (2004).

_____

*Corresponding author: xzsang@gmail.com